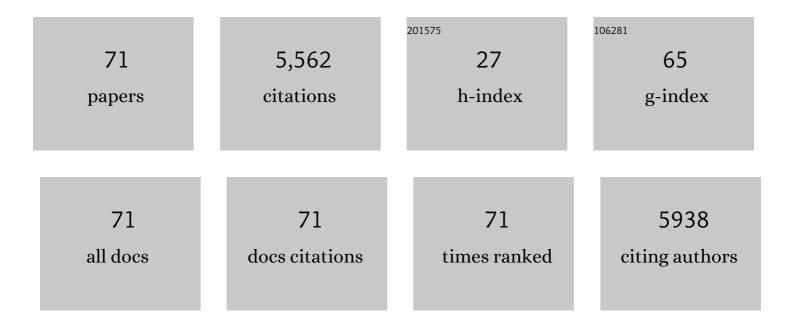
Zhiqiang Xiao

List of Publications by Year in descending order

Source: https://exaly.com/author-pdf/1554811/publications.pdf Version: 2024-02-01



#	Article	IF	CITATIONS
1	Greening of the Earth and its drivers. Nature Climate Change, 2016, 6, 791-795.	8.1	1,675
2	Increased atmospheric vapor pressure deficit reduces global vegetation growth. Science Advances, 2019, 5, eaax1396.	4.7	755
3	Use of General Regression Neural Networks for Generating the GLASS Leaf Area Index Product From Time-Series MODIS Surface Reflectance. IEEE Transactions on Geoscience and Remote Sensing, 2014, 52, 209-223.	2.7	486
4	A long-term Global LAnd Surface Satellite (GLASS) data-set for environmental studies. International Journal of Digital Earth, 2013, 6, 5-33.	1.6	385
5	Long-Time-Series Global Land Surface Satellite Leaf Area Index Product Derived From MODIS and AVHRR Surface Reflectance. IEEE Transactions on Geoscience and Remote Sensing, 2016, 54, 5301-5318.	2.7	297
6	The Global Land Surface Satellite (GLASS) Product Suite. Bulletin of the American Meteorological Society, 2021, 102, E323-E337.	1.7	203
7	Characterization and intercomparison of global moderate resolution leaf area index (LAI) products: Analysis of climatologies and theoretical uncertainties. Journal of Geophysical Research C: Biogeosciences, 2013, 118, 529-548.	1.3	149
8	A Multiscale and Hierarchical Feature Extraction Method for Terrestrial Laser Scanning Point Cloud Classification. IEEE Transactions on Geoscience and Remote Sensing, 2015, 53, 2409-2425.	2.7	138
9	Global Land Surface Fractional Vegetation Cover Estimation Using General Regression Neural Networks From MODIS Surface Reflectance. IEEE Transactions on Geoscience and Remote Sensing, 2015, 53, 4787-4796.	2.7	137
10	Real-time retrieval of Leaf Area Index from MODIS time series data. Remote Sensing of Environment, 2011, 115, 97-106.	4.6	96
11	Evaluation of four long time-series global leaf area index products. Agricultural and Forest Meteorology, 2017, 246, 218-230.	1.9	90
12	Retrieval of leaf area index using temporal, spectral, and angular information from multiple satellite data. Remote Sensing of Environment, 2014, 145, 25-37.	4.6	83
13	Estimating the fraction of absorbed photosynthetically active radiation from the MODIS data based GLASS leaf area index product. Remote Sensing of Environment, 2015, 171, 105-117.	4.6	77
14	A Temporally Integrated Inversion Method for Estimating Leaf Area Index From MODIS Data. IEEE Transactions on Geoscience and Remote Sensing, 2009, 47, 2536-2545.	2.7	66
15	Evaluation of MODIS and two reanalysis aerosol optical depth products over AERONET sites. Atmospheric Research, 2019, 220, 75-80.	1.8	64
16	Bayesian Method for Building Frequent Landsat-Like NDVI Datasets by Integrating MODIS and Landsat NDVI. Remote Sensing, 2016, 8, 452.	1.8	61
17	Estimation of Global Vegetation Productivity from Global LAnd Surface Satellite Data. Remote Sensing, 2018, 10, 327.	1.8	58
18	Long-Term Global Land Surface Satellite (GLASS) Fractional Vegetation Cover Product Derived From MODIS and AVHRR Data. IEEE Journal of Selected Topics in Applied Earth Observations and Remote Sensing, 2019, 12, 508-518.	2.3	41

ZHIQIANG XIAO

#	Article	IF	CITATIONS
19	Estimating the Fractional Vegetation Cover from GLASS Leaf Area Index Product. Remote Sensing, 2016, 8, 337.	1.8	37
20	GLASS Daytime All-Wave Net Radiation Product: Algorithm Development and Preliminary Validation. Remote Sensing, 2016, 8, 222.	1.8	36
21	Consistent estimation of multiple parameters from MODIS top of atmosphere reflectance data using a coupled soil-canopy-atmosphere radiative transfer model. Remote Sensing of Environment, 2016, 184, 40-57.	4.6	36
22	A Framework for Consistent Estimation of Leaf Area Index, Fraction of Absorbed Photosynthetically Active Radiation, and Surface Albedo from MODIS Time-Series Data. IEEE Transactions on Geoscience and Remote Sensing, 2015, 53, 3178-3197.	2.7	35
23	Evaluation of Three Long Time Series for Global Fraction of Absorbed Photosynthetically Active Radiation (FAPAR) Products. IEEE Transactions on Geoscience and Remote Sensing, 2018, 56, 5509-5524.	2.7	33
24	Surface Daytime Net Radiation Estimation Using Artificial Neural Networks. Remote Sensing, 2014, 6, 11031-11050.	1.8	32
25	Evaluation of topographic effects on multiscale leaf area index estimation using remotely sensed observations from multiple sensors. ISPRS Journal of Photogrammetry and Remote Sensing, 2019, 154, 176-188.	4.9	29
26	New Global MuSyQ GPP/NPP Remote Sensing Products From 1981 to 2018. IEEE Journal of Selected Topics in Applied Earth Observations and Remote Sensing, 2021, 14, 5596-5612.	2.3	29
27	Reconstruction of Long-Term Temporally Continuous NDVI and Surface Reflectance From AVHRR Data. IEEE Journal of Selected Topics in Applied Earth Observations and Remote Sensing, 2017, 10, 5551-5568.	2.3	28
28	Evaluation and Comparison of Light Use Efficiency and Gross Primary Productivity Using Three Different Approaches. Remote Sensing, 2020, 12, 1003.	1.8	26
29	Reconstruction of Satellite-Retrieved Land-Surface Reflectance Based on Temporally-Continuous Vegetation Indices. Remote Sensing, 2015, 7, 9844-9864.	1.8	25
30	A Method for Consistent Estimation of Multiple Land Surface Parameters From MODIS Top-of-Atmosphere Time Series Data. IEEE Transactions on Geoscience and Remote Sensing, 2017, 55, 5158-5173.	2.7	25
31	Simultaneous inversion of multiple land surface parameters from MODIS optical–thermal observations. ISPRS Journal of Photogrammetry and Remote Sensing, 2017, 128, 240-254.	4.9	24
32	Retrieval of Leaf Area Index (LAI) and Fraction of Absorbed Photosynthetically Active Radiation (FAPAR) from VIIRS Time-Series Data. Remote Sensing, 2016, 8, 351.	1.8	23
33	Spatially and Temporally Complete Satellite Soil Moisture Data Based on a Data Assimilation Method. Remote Sensing, 2016, 8, 49.	1.8	22
34	Performance Evaluation of Machine Learning Methods for Leaf Area Index Retrieval from Time-Series MODIS Reflectance Data. Sensors, 2017, 17, 81.	2.1	20
35	Validation of the Surface Daytime Net Radiation Product From Version 4.0 GLASS Product Suite. IEEE Geoscience and Remote Sensing Letters, 2019, 16, 509-513.	1.4	19
36	GBRT-Based Estimation of Terrestrial Latent Heat Flux in the Haihe River Basin from Satellite and Reanalysis Datasets. Remote Sensing, 2021, 13, 1054.	1.8	16

ZHIQIANG XIAO

#	Article	IF	CITATIONS
37	Simultaneous Estimation of Leaf Area Index, Fraction of Absorbed Photosynthetically Active Radiation, and Surface Albedo From Multiple-Satellite Data. IEEE Transactions on Geoscience and Remote Sensing, 2017, 55, 4334-4354.	2.7	14
38	Evaluation of the version 5.0 global land surface satellite (GLASS) leaf area index product derived from MODIS data. International Journal of Remote Sensing, 2020, 41, 9140-9160.	1.3	14
39	Multiscale Estimation of Leaf Area Index from Satellite Observations Based on an Ensemble Multiscale Filter. Remote Sensing, 2016, 8, 229.	1.8	13
40	Generation of High Resolution Vegetation Productivity from a Downscaling Method. Remote Sensing, 2018, 10, 1748.	1.8	13
41	Simulating spatially distributed solar-induced chlorophyll fluorescence using a BEPS-SCOPE coupling framework. Agricultural and Forest Meteorology, 2020, 295, 108169.	1.9	13
42	Variational retrieval of leaf area index from MODIS time series data: examples from the Heihe river basin, north-west China. International Journal of Remote Sensing, 2012, 33, 730-745.	1.3	11
43	Extended Data-Based Mechanistic Method for Improving Leaf Area Index Time Series Estimation with Satellite Data. Remote Sensing, 2017, 9, 533.	1.8	11
44	Simultaneous Estimation of Multiple Land-Surface Parameters From VIIRS Optical-Thermal Data. IEEE Geoscience and Remote Sensing Letters, 2018, 15, 156-160.	1.4	10
45	Sequential Method with Incremental Analysis Update to Retrieve Leaf Area Index from Time Series MODIS Reflectance Data. Remote Sensing, 2014, 6, 9194-9212.	1.8	9
46	A Multiscale Assimilation Approach to Improve Fine-Resolution Leaf Area Index Dynamics. IEEE Transactions on Geoscience and Remote Sensing, 2019, 57, 8153-8168.	2.7	9
47	Exploration of Machine Learning Techniques in Emulating a Coupled Soil–Canopy–Atmosphere Radiative Transfer Model for Multi-Parameter Estimation From Satellite Observations. IEEE Transactions on Geoscience and Remote Sensing, 2019, 57, 8522-8533.	2.7	8
48	Data-based mechanistic modelling and validation for leaf area index estimation using multi-angular remote-sensing observation time series. International Journal of Remote Sensing, 2014, 35, 4655-4672.	1.3	7
49	Observed Vegetation Greening and Its Relationships with Cropland Changes and Climate in China. Land, 2020, 9, 274.	1.2	7
50	Interannual variation of gross primary production detected from optimal convolutional neural network at multiâ€ŧimescale water stress. Remote Sensing in Ecology and Conservation, 2022, 8, 409-425.	2.2	7
51	A Data Assimilation Method for Simultaneously Estimating the Multiscale Leaf Area Index From Time-Series Multi-Resolution Satellite Observations. IEEE Transactions on Geoscience and Remote Sensing, 2019, 57, 9344-9361.	2.7	6
52	The 4SAILT Model: An Improved 4SAIL Canopy Radiative Transfer Model for Sloping Terrain. IEEE Transactions on Geoscience and Remote Sensing, 2021, 59, 5515-5525.	2.7	6
53	A 250 m resolution global leaf area index product derived from MODIS surface reflectance data. International Journal of Remote Sensing, 2022, 43, 1409-1429.	1.3	6
54	Simplified Priestley–Taylor Model to Estimate Land-Surface Latent Heat of Evapotranspiration from Incident Shortwave Radiation, Satellite Vegetation Index, and Air Relative Humidity. Remote Sensing, 2021, 13, 902.	1.8	5

ZHIQIANG XIAO

#	Article	IF	CITATIONS
55	Evaluation of county-level poverty alleviation progress by deep learning and satellite observations. Big Earth Data, 2021, 5, 576-592.	2.0	5
56	An airborne multi-angle power line inspection system. , 2007, , .		4
57	Consistent retrieval of multiple parameters from GOES-R top of atmosphere reflectance data. International Journal of Remote Sensing, 2020, 41, 7931-7957.	1.3	4
58	Multiscale approach for fusing leaf area index estimates from multiple sensors. Proceedings of SPIE, 2007, , .	0.8	3
59	Leaf area index estimation from MODIS data using the ensemble Kalman smoother method. , 2010, , .		3
60	Combining MODIS and AMSR-E observations to improve MCD43A3 short-time snow-covered Albedo estimation. Hydrological Processes, 2014, 28, 570-580.	1.1	3
61	Exploring Topographic Effects on Surface Parameters Over Rugged Terrains at Various Spatial Scales. IEEE Transactions on Geoscience and Remote Sensing, 2022, 60, 1-16.	2.7	3
62	Retrieval of the Leaf Area Index from Visible Infrared Imaging Radiometer Suite (VIIRS) Surface Reflectance Based on Unsupervised Domain Adaptation. Remote Sensing, 2022, 14, 1826.	1.8	3
63	An Optical–Thermal Surface–Atmosphere Radiative Transfer Model Coupling Framework With Topographic Effects. IEEE Transactions on Geoscience and Remote Sensing, 2022, 60, 1-12.	2.7	2
64	SIFT: Modeling Solar-Induced Chlorophyll Fluorescence Over Sloping Terrain. IEEE Geoscience and Remote Sensing Letters, 2022, 19, 1-5.	1.4	2
65	Evaluation of Global Fraction of Absorbed Photosynthetically Active Radiation (FAPAR) Products at 500 m Spatial Resolution. Remote Sensing, 2022, 14, 3304.	1.8	2
66	Multiparameter Estimation From Landsat Observations With Topographic Consideration. IEEE Transactions on Geoscience and Remote Sensing, 2021, 59, 7353-7369.	2.7	1
67	A Canopy Radiative Transfer Model Considering Leaf Dorsoventrality. IEEE Transactions on Geoscience and Remote Sensing, 2022, 60, 1-11.	2.7	1
68	Estimation of Global Net Primary Productivity from 1981 to 2018 with Remote Sensing Data. , 2020, , .		1
69	Land surface parameters retrieval using time series remotely sensed observations. , 2007, , .		0
70	Simultaneous Estimation of LAI and Dynamic Model Parameters Using Dual EnKF from Time Series MODIS Data. , 2010, , .		0
71	Daily High-Resolution Land Surface Freeze/Thaw Detection Using Sentinel-1 and AMSR2 Data. Remote Sensing, 2022, 14, 2854.	1.8	0